Table 1. Fundamental frequencies of the inverted pendulum.

	X [mHz]	Y [mHz]	θ [Hz]
NM1	50	60	0.50
EM1	150	50	0.54
NM2	30	60	0.52
EM2	50	70	0.50

driving signals must be diagonalized to the directions of X, Y and θ. Six channels are assigned to the ADC inputs of the digital controller for the accelerometers and the position sensors. Analog anti-aliasing filters (AAF) are mounted in front of the ADC inputs. Three channels are assigned to the DAC outputs for the actuators. The main process of the digital controller is the diagonalization and filtering of the input signals, as well as generating control voltages on the three actuators corresponding to three virtual actuators acting on each of the eigenmodes of the IP. First, the diagonalization matrix was decided using natural modes which appear in the measured transfer functions from each actuator to each sensor. Second, optimal servo filters were designed using the measured transfer functions from a diagonalized virtual actuator to a virtual sensor. The loop rate of the process is 250 Hz. The unity gain frequency of the open loop is at 2 Hz. Additionally, there are a global control loop for the cavity length and a damping control loop for excited torsion modes using a differential photo sensor (PS) and the virtual actuator acting on θ. These torsion modes are due to the moment of inertia of the payload suspended by a single wire from the IP. The fundamental mode has a resonant frequency of ∼40 mHz and a long settle time of ∼1000 s.

The other is the platform and test-mass (PF-TM) control shown schematically on the right side of figure 2. Signals of the test-mass rotation (pitch and yaw) detected by a local optical lever (OL) are fed back to the test-mass actuators. The loop rate of this process is 1 kHz. The unity gain frequency of the open loop is at 2–3 Hz. After the cavity is locked, the sensing signals are replaced by global signals from the interferometer acquired by the wave front sensing (WFS) method [19, 20]. We could successfully change the control signals from the optical lever to the WFS without the loss of lock. Additionally, there are control loops for the platform. At present, this function is used only to apply DC offsets for the initial alignment of the test-mass.

2.3. Characteristics of the inverted pendulum

The fundamental frequencies of the inverted pendulum (IP), which characterize the quality of each SAS, are shown in table 1. Most of the horizontal modes (X and Y) were tuned to be lower than 100 mHz except for EM1 in which an asymmetry of the elastic spring components of the IP caused the large splitting of the modes. The frequencies of rotational mode (θ) are ∼0.5 Hz. The natural quality factor Q of the horizontal modes was very small (1 or less). This property causes the $1/f$ (where f is the frequency) behavior of the vibration isolation function. As a result, the attenuation from the ground motion of the IP was about −25 dB at 1 Hz. A prototype TAMA SAS had Q of ∼10 at 50 mHz [9]. It is likely that vacuum-compatible stiff wires used for electric signals added mechanical loss.

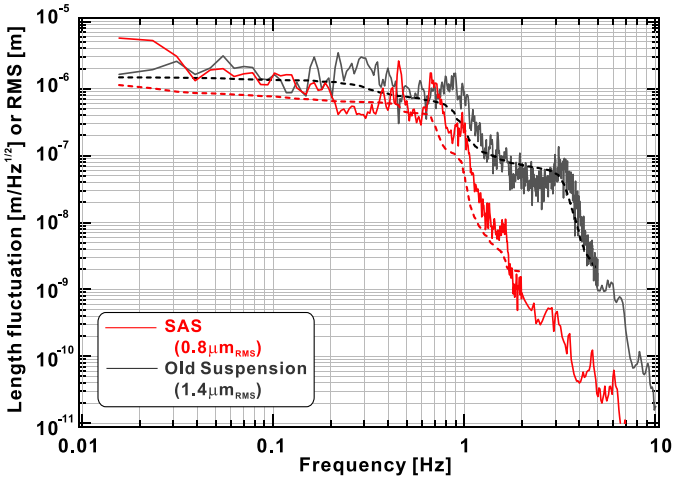

Figure 3. Length fluctuation of the 300 m cavity measured by the feedback signals to lock the cavity. The spectrum density and RMS integrated from 50 mHz are indicated by solid line and dash line, respectively.

3. Confirmation of performance

3.1. Configurations of the interferometer

We installed the SAS one by one and confirmed its performance using the TAMA interferometer step-by-step: Step-1, one arm; Step-2, locked Fabry–Perot (FP); Step-3, recycled Fabry–Perot Michelson interferometer (FPMI).

In Step-1, one arm with the SAS was compared with the other arm with the old suspension. The length fluctuation of the arm cavity was measured by the feedback signal fed to the laser in order to lock the cavity.

In Step-2, each arm cavity with the SAS was locked differentially. We call this configuration the locked FP. The inline arm cavity was locked by actuating the laser frequency for stabilization of the light source, while the perpendicular arm cavity was locked to this stabilized light by actuating the front mirror of the perpendicular arm, so-called mass-lock. Since the power recycling mirror was misaligned, the light power was very small.

Step-3 is close to the full configuration with power recycling. The recycling mirror and Michelson part are locked using signals demodulated at the third-harmonic frequency [21]. Only the signal for the Michelson part is changed to signal demodulated at the first-harmonic frequency after the lock acquisition.

3.2. Length performance

The length fluctuation of the cavity was confirmed in the Step-1 configuration. The global control for the cavity length was not working. The arm with the SAS showed reduced fluctuation above 0.1 Hz as compared with the arm with the old suspension, as shown in figure 3. Attenuation better than $1/f^5$ was achieved above 1 Hz. The mechanical resonances of multi-pendulum around 1 Hz and micro-seismic motion around 0.3 Hz are successfully damped by the digital servo system. RMS fluctuation integrated from 50 mHz was 0.8 μm with the SAS. This is comparable with RMS of 1.4 μm with the old suspension.

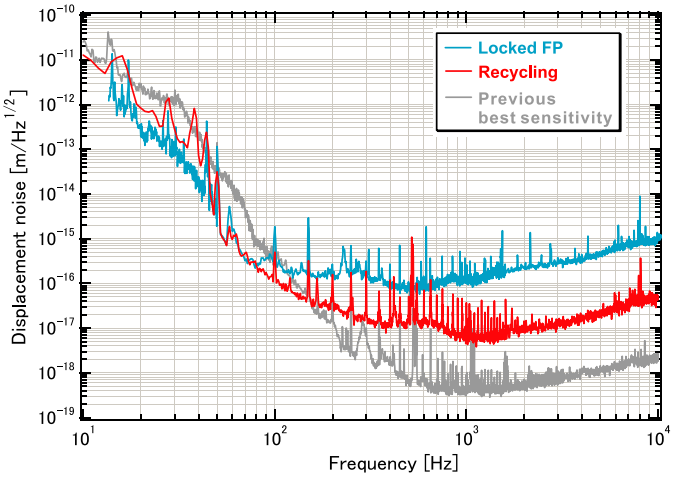

Figure 4. Sensitivity of TAMA300 with the SAS in Step-2 configuration (locked FP) and Step-3 configuration (recycling). The previous best sensitivity is also shown. Please note that the worsened sensitivity above 150 Hz is due to the incomplete commissioning of the interferometer. The SAS has no effect above 100 Hz.

Improvement of the displacement noise at 0.1–100 Hz was confirmed in the Step-2 configuration as compared with the previous best sensitivity (figure 4). The sensitivity around 1 kHz was far from the best one because of small light power.

In the Step-3 configuration, the sensitivity of around 1 kHz was close to the best one as shown in figure 4. The improved frequency region was extended to 150 Hz. Please note that the worsened sensitivity above 150 Hz is due to the incomplete commissioning of the interferometer. The light power at the dark port was not large enough to obtain the sensitivity consistent with the best one. The SAS has no effect above 100 Hz.

An alignment noise was still dominant at 10–50 Hz. One thing, however, is certain: the signals acquired by the WFS are larger than the signals acquired by the local optical lever. The WFS may couple to jitters of the incident beam to the arm cavity. Therefore, a common mode signal should be fed back not to the test-mass mirrors but to the incident beam. We need a new servo topology to solve this problem.

3.3. Angular performance

We confirmed the angular fluctuation of the test-mass using an optical lever. The fluctuation with the SAS showed improvement above 1 Hz as compared with the fluctuation with the old suspension as shown in figure 5. Sensing noise of the optical lever is lying around 10^{-9} rad Hz$^{-1/2}$. Although the uncontrolled RMS fluctuation with the SAS (12μ rad for yaw) was larger than the fluctuation with the old suspension (1.0μ rad), we could set the bandwidth of the alignment control servo to 2–3 Hz. It was 10–20 Hz previously. The many resonant peaks below 3 Hz, due to the multi-pendulum, were damped using a servo filter with many pole–zero pairs. It is difficult to construct such a filter by an analog circuit at frequencies below 1 Hz. The residual RMS of angular fluctuation was 0.2 μrad with the control. This will result in a reduction of the noise due to the alignment control system which limited the former sensitivity of TAMA300.

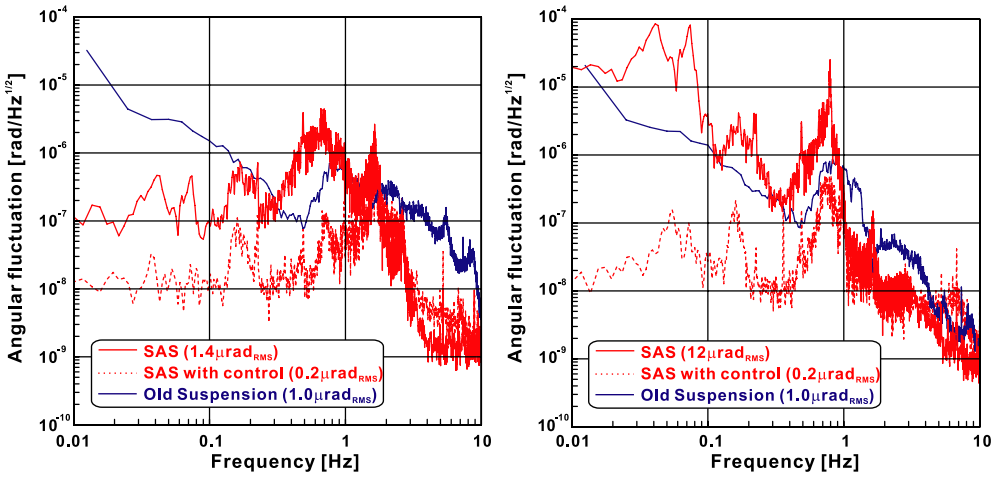

Figure 5. Angular fluctuation of the north–south front test-mass (NM2) measured by an optical lever. The spectrum density in the pitch direction (left) and in the yaw direction (right) are shown, respectively.

4. Summary

Installation of the SAS into TAMA300 was completed. The recycled FPMI was successfully locked using the established control system for the SAS. The length fluctuation of the 300 m cavity was improved above 0.1 Hz owing to the SAS. The improved angular fluctuation of the test-mass will result in a reduction of the alignment noise.

Acknowledgments

This work was supported by the Grant-in-Aid for Scientific Research of the Ministry of Education, Culture, Sports, Science and Technology (09NP0801 in Creative Scientific Research and 415 in Priority Areas). Developments of the TAMA SAS were supported by the Advanced Technology Center of National Astronomical Observatory of Japan and the U.S. National Science Foundation under Cooperative Agreement No PHY-0107417.

References

[1] Ando M and the TAMA Collaboration 2005 *Class. Quantum Grav.* **22** S881
[2] Kuroda K and the LCGT Collaboration 2006 *Class. Quantum Grav.* **23** S215
[3] Lück H *et al* 2006 *Class. Quantum Grav.* **23** S71
[4] Sigg A 2006 *Class. Quantum Grav.* **23** S51
[5] Acernese F *et al* 2006 *Class. Quantum Grav.* **23** S63
[6] Akutsu T *et al* 2006 *Phys. Rev.* D **74** 122002
[7] Takahashi R and the TAMA Collaboration 2004 *Class. Quantum Grav.* **21** S403
[8] Márka S *et al* 2002 *Class. Quantum Grav.* **19** 1605
[9] Takamori A 2002 *PhD Thesis* LIGO-P-030049-00-R http://admdbsrv.ligo.caltech.edu/dcc/
[10] Takahashi R *et al* 2002 *Rev. Sci. Instrum.* **73** 2428
[11] Takahashi R *et al* 2002 *Class. Quantum Grav.* **19** 1599
[12] Braccini S *et al* 2005 *Astropart. Phys.* **23** 557
[13] Takamori A *et al* 2007 *Nucl. Instrum. Methods* A **582** 683

[14] Cella G *et al* 2005 *Nucl. Instrum. Methods* A **540** 502
[15] Takamori A *et al* 2002 *Class. Quantum Grav.* **19** 1615
[16] Bertolini A *et al* 2006 *Nucl. Instrum. Methods* A **556** 616
[17] Tariq H *et al* 2002 *Nucl. Instrum. Methods* A **489** 570
[18] Wang C *et al* 2002 *Nucl. Instrum. Methods* A **489** 563
[19] Morrison E *et al* 1994 *Appl. Opt.* **33** 5037
[20] Morrison E *et al* 1994 *Appl. Opt.* **33** 5041
[21] Arai K *et al* 2000 *Phys. Lett.* A **273** 15